remote sensing

MDPI

Article

Medium-Resolution Multispectral Data from Sentinel-2 to Assess the Damage and the Recovery Time of Late Frost on Vineyards

Alessia Cogato [1,*], Franco Meggio [2], Cassandra Collins [3] and Francesco Marinello [1]

[1] Department of Land, Environmental, Agriculture and Forestry, University of Padova, 35020 Legnaro (PD), Italy; francesco.marinello@unipd.it
[2] Department of Agronomy, Food, Natural Resources, Animals and the Environment, University of Padova, 35020 Legnaro (PD), Italy; franco.meggio@unipd.it
[3] School of Agriculture, Food and Wine, The University of Adelaide, Waite Research Institute, Glen Osmond, Adelaide, SA 5064, Australia; cassandra.collins@adelaide.edu.au
* Correspondence: alessia.cogato.1@phd.unipd.it

Received: 30 April 2020; Accepted: 9 June 2020; Published: 11 June 2020

Abstract: In a climate-change context, the advancement of phenological stages may endanger viticultural areas in the event of a late frost. This study evaluated the potential of satellite-based remote sensing to assess the damage and the recovery time after a late frost event in 2017 in northern Italian vineyards. Several vegetation indices (VIs) normalized on a two-year dataset (2018–2019) were compared over a frost-affected area (F) and a control area (NF) using unpaired two-sample *t*-test. Furthermore, the must quality data (total acidity, sugar content and pH) of F and NF were analyzed. The VIs most sensitive in the detection of frost damage were Chlorophyll Absorption Ratio Index (CARI), Enhanced Vegetation Index (EVI), and Modified Triangular Vegetation Index 1 (MTVI1) (−5.26%, −16.59%, and −5.77% compared to NF, respectively). The spectral bands Near-Infrared (NIR) and Red Edge 7 were able to identify the frost damage (−16.55 and −16.67% compared to NF, respectively). Moreover, CARI, EVI, MTVI1, NIR, Red Edge 7, the Normalized Difference Vegetation Index (NDVI) and the Modified Simple Ratio (MSR) provided precise information on the full recovery time (+17.7%, +22.42%, +29.67%, +5.89%, +5.91%, +16.48%, and +8.73% compared to NF, respectively) approximately 40 days after the frost event. The must analysis showed that total acidity was higher (+5.98%), and pH was lower (−2.47%) in F compared to NF. These results suggest that medium-resolution multispectral data from Sentinel-2 constellation may represent a cost-effective tool for frost damage assessment and recovery management.

Keywords: spring frost; multispectral remote sensing; vegetation indices; grapevine; frost damage; *Vitis vinifera*

1. Introduction

In the current context of a warming climate, late frost events may affect viticulture more frequently, due to a forward shift of phenological development [1]. Late frost events pose a severe threat to grapevine cultivation in frost-prone viticultural areas. For example, serious damage occurred on average, twice every ten years in Poland [2]. Frost events during budbreak have significantly increased in Spain, France, and the UK during the period, 1980–2010 [3]. The length of the frost risk season was shown to have increased by four weeks in South Australia [4]. Climate model projections show earlier budbreak and flowering [3,5] which has consequently increased the impact of frost events in central Europe [3,6] and the UK [7].

In spring 2017 an advective frost from the Arctic reached central and Western Europe, affecting most Italian wine regions. The incursion of dry artic air followed an unusually warm period, which had caused advanced budbreak in grapevine. The injuries to the young shoots, especially in the low-lying areas, were very severe. In Vicenza province (Veneto Region), local authorities estimated 60 to 80% of vineyards in this area were damaged.

Late frost can cause severe damage to a grapevine as a buds resistance to freezing decreases with advancing phenological development and increased water content [8–10]. Injuries can occur to buds, young shoots, inflorescence, and leaves. When major losses occur, the basal and secondary buds can respond by bursting to produce new shoots. Typically, the new shoots are less fruitful, leading to crop losses [10,11].

When late frost damage occurs, prompt assessment and quantification of the damage is crucial to support reactive and effective decision-making. Although farms have some management options to reduce the exposure to adverse weather events, the farmers' risk is usually managed with crop insurance. Thus, effective damage assessment also concerns the insurance industry. The conventional methods for damage assessment are based on visual or thermal field examination of vines. For example, oxidative browning allows for injured tissue detection as they turn brown after releasing the phenolic compounds [12]. Thermal analysis detects the latent heat produced by frozen tissues due to the water transition from liquid to solid [13,14].

However, these methods are time-consuming, costly, and unsuitable for large areas, thus impeding rapid damage assessment. Several authors suggested the use of satellite data as a tool for more cost-effective agricultural damage assessment [15–17].

Alternative approaches, such as spectral image-based analysis, have been shown to have potential to assess frost damage on a large scale with acceptable accuracy. The normalized difference vegetation index (NDVI) derived from low spatial-resolution data (HJ-1A/1B, moderate-resolution imaging spectroradiometer - MODIS) and medium resolution imaging spectrometer - MERIS) showed significant correlations with frost damage indices in oilseed rape in China [18,19]. Similarly, NDVI computed using MODIS imagery was found to correlate with the severity of late frost damage to Aspen forests in Utah, USA [20]. Hyperspectral imaging from handheld spectrometers was used to estimate frost damage in winter wheat in China [21] and oilseed rape in Canada [22]. Su et al. [23] derived a Digital Surface Model from a high definition red-green-blue (RGB) camera mounted on an Unmanned Aerial Vehicle (UAV) to identify missing or affected vines as a result of frost events in China. Despite their potential, the previous approaches are not suitable to detect large-scale weather events affecting vineyards. On the one hand, the low spatial resolution of MODIS imagery (250 m) would not provide sufficiently reliable information on this crop, as cultivation is often fragmented. On the other hand, the deployment of UAVs has some critical drawbacks due to high costs and the legal frameworks that regulate and restrict flight operations.

The advent of free imagery archives, e.g., the United States Geological Survey (USGS) Earth Explorer or the European Space Agency (ESA) Sentinel Mission, allows the implementation of multispectral analysis for large areas. However, the spatial resolution of these images is not high enough to enable the discrimination between rows and inter-rows of the vineyards, and as such limit their application to this crop [24]. Previous research has highlighted remarkable consistency between vegetation indices (VIs) derived from high- and medium-spatial resolution images [24–27]. Open source medium-resolution datasets were used in vineyards to determine leaf area index (LAI) [28], predict wine yield [29,30] and assess heat stress [24]. However, to date, medium-spatial resolution imagery has not been used to evaluate late frost damage in vineyards.

The goal of this study was to test the hypothesis that the reflectance values of specific spectral regions and the VIs derived from Sentinel-2 imagery can identify frost damage in vineyards and assess the recovery time.

The objectives were therefore to (i) identify the VIs/spectral bands that can be used as damage markers in frost-affected vineyards, and (ii) estimate the recovery time of vines affected by frost damage.

2. Materials and Methods

2.1. Site Data

The study was conducted in an area belonging to a winegrowers' cooperative located in the province of Vicenza, in the north-east of Italy (45°23′29.30′′ N and 11°24′15.36′′ E). Onto undertake this study *Vitis vinifera* cv. Garganega, a white variety mainly cultivated in the provinces of Vicenza and Verona was used. A severe late frost occurred on 19 April 2017 (Figure 1) after an unusually warm period in the weeks preceding the frost event which led to increased vegetative growth. The large temperature drop due to the frosty led to severe damage over an extensive area. According to the Biologische Bundesanstalt, Bundessortenamt and CHemical industry BBCH scale [31], the phenological growth stage of Garganega on the 19th of April was 11 (first leaf separated from shoot tip), about 15 days earlier than usual.

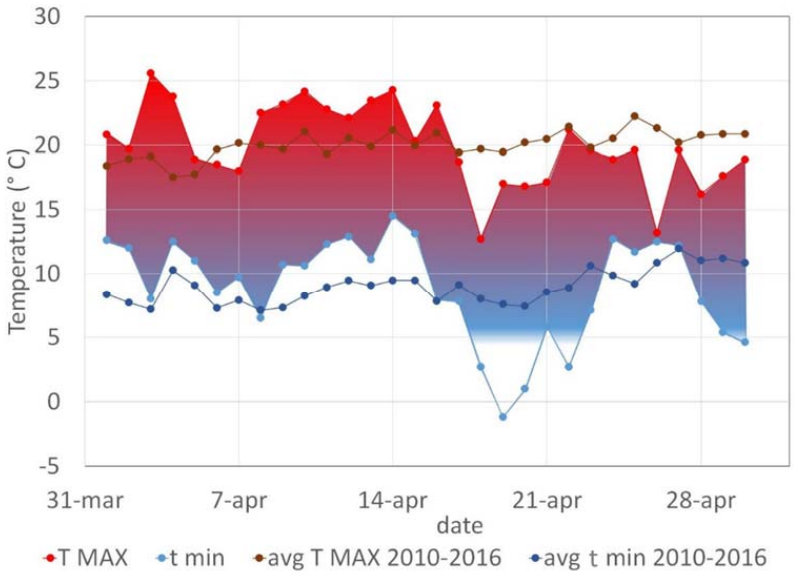

Figure 1. Curve of daily maximum and minimum temperature during the period April–June 2017 and the reference period 2010–2016. The daily air temperature data were provided by Agenzia Regionale per la Prevenzione e Protezione Ambientale ARPA Veneto and are available online https://www.arpa.veneto.it/bollettini/storico/2017/0105_2017_TEMP.htm.

In an area of 20 km^2, six plots located in commercial vineyards, were identified: three were affected by frost damage (F), and three were unaffected and used as controls (NF) for a total area of 4.96 ha and 11.43 ha for F and NF, respectively (Figure 2). The vines were trained to the traditional "Pergola" training system with a continuous horizontal layer of foliage at full development. The interrow of five plots was sown with a perennial cover crop, comprised of a mixture of *Poaceae*, the interrow of the sixth plot was bare (no vegetation). Pre-emergent herbicides were applied at the end of March, while the cover crop was mowed one week before the frost event. Table 1 shows the main characteristics of the plots. Figure 3 shows the frost damage on the vines.

Table 1. Characteristics of the sample plots.

Plot ID	Area (ha)	Row Spacing	Interrow Management
F1	1.78	5.0	Cover crop
F2	1.66	4.2	Bare soil
F3	1.52	4.5	Cover crop
NF1	2.78	4.5	Cover crop
NF2	3.72	4.5	Cover crop
NF3	4.93	5.0	Cover crop

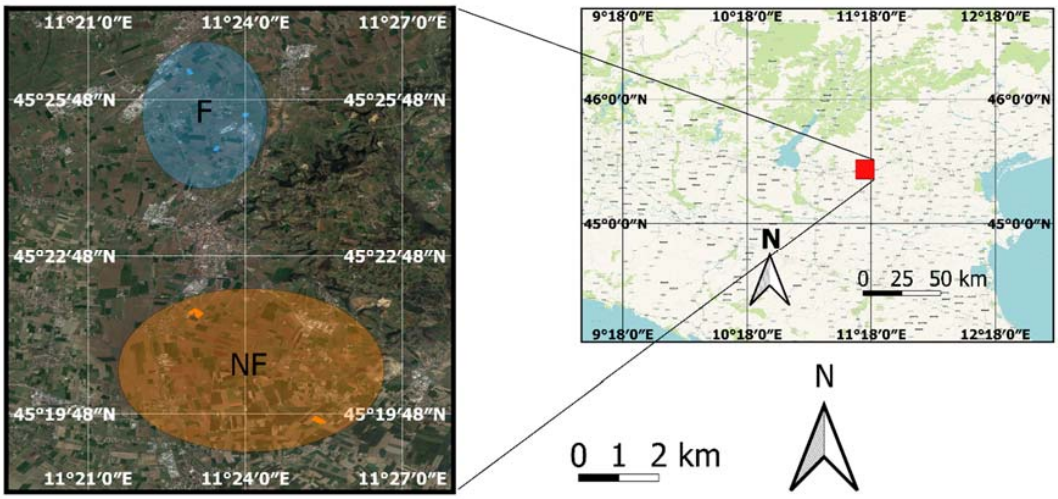

Figure 2. The study area is in Veneto Region, province of Vicenza. The north–south distance of frost-affected vineyards (F) and control area (NF) is approx. 10 km.

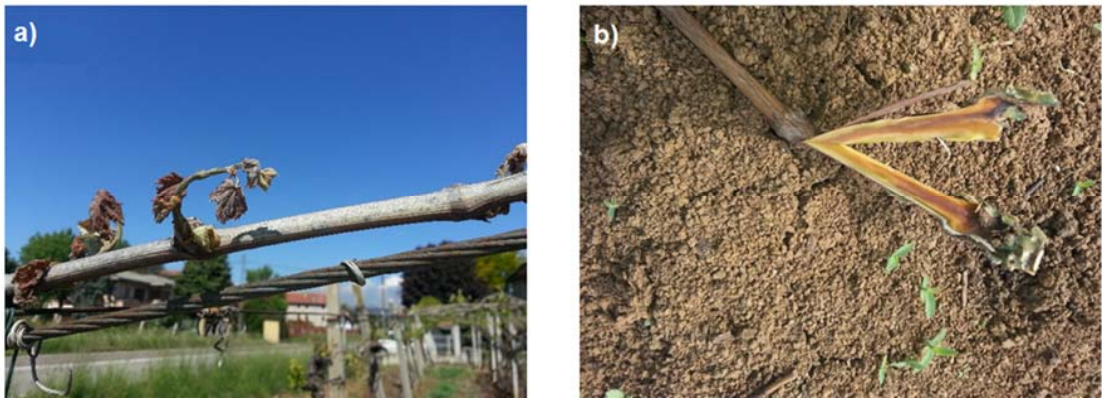

Figure 3. Frost damage affected both (**a**) green and (**b**) woody tissues.

2.2. Remote Sensing Data

Five Sentinel-2 images were acquired from 14 April to 23 June 2017. Within the total amount of eight images available in the Copernicus Open-Access Hub, two (24 April and 5 May) were unusable because cloud coverage was very high (around 90%). A third image (13 June) was considered redundant, given the availability of two images taken at very close dates. Within the same two-month period, four images were acquired in 2018 and four in 2019 (Table 2). The aim was to only use images with very close dates to the ones selected for 2017. The available images close to the 24th of May were characterized by very high cloud coverage. The analysis aimed to assess the frost stress indicators derived from multispectral data and provide an evaluation of the recovery time of the F vineyards compared to the NF ones, based on the comparison between the trend of selected VIs and spectral bands.

Table 2. List of the satellite images used in this study (NA = not available).

Image ID.	S1	S2	S3	S4	S5
	14/04/2017	14/05/2017	24/05/2017	03/06/2017	23/06/2017
	14/04/2018	19/05/2018	NA	03/06/2018	18/06/2018
	19/04/2019	14/05/2019	NA	03/06/2019	23/06/2019

The Sentinel-2 platform carries a multispectral sensor covering 13 spectral bands, from 0.443 to 2.190 µm. Four visible and near-infrared bands are available at a 10 m spatial resolution, six red-edge/shortwave-infrared bands at 20 m, while three atmospheric correction bands have 60 m resolution. The atmospheric correction of 2017 images (S1–S5) was performed using the SEN2COR tool. The algorithm is available in the Sentinel Application Platform (SNAP) toolbox. SEN2COR is a Level-2A (L2A) processor which corrects single-date Sentinel-2 Level-1C products from the effects of the atmosphere [32]. After correction, every spectral band image was cropped with an inner buffer of 10 m, creating a mask with QGIS 2.4 (http://www.qgis.org/). This step aimed to avoid the border effects [33]. In the case of CARI, which has a spatial resolution of 20 m, the cropping was done by selecting only the pixels entirely included in the same mask used for the 10 m spatial resolution VIs. From March 2018, Level-2A (BOA reflectance–atmospherically corrected) products were made available for download. Therefore, images from 2018 and 2019 were not processed with the SEN2COR tool.

Seven VIs were used in this study. VIs, such as NDVI, EVI, GNDVI and the Soil Adjusted Vegetation Index (SAVI) were chosen based on previous studies on the spectral response of crops to frost damage [18,19,22]. Given the lack of research on the correlation between multispectral features and frost damage, this investigation explored for the first time different VIs and the reflectance of five spectral bands (bands 5, 6, 7, 8, and 11). The list of the spectral bands and the VIs employed in this study are reported in Tables 3 and 4. The computation of VIs and spectral bands was performed with R statistical software (Version 3.5.2, RStudio Version 1.0.463) using a custom script. Since the computation of CARI involved the red-edge spectral band, with a spatial resolution of 20 m, this VI was calculated using 20 m resolution for red and green spectral bands.

Table 3. Sentinel-2 spectral bands used in this study.

Sentinel-2 Band	Central Wavelength (nm)	Bandwidth (nm)	Spatial Resolution (m)
Band 2—Blue	490	66	10–20
Band 3—Green	560	36	10–20
Band 4—Red	665	31	10–20
Band 5—Vegetation Red Edge	705	15	20
Band 6—Vegetation Red Edge	740	15	20
Band 7—Vegetation Red Edge	783	20	20
Band 8—Near Infrared (NIR)	842	115	10
Band 11—Short Wave Infrared (SWIR)	1610	90	20

Table 4. List of the VIs used in this study.

Index	Acronym	Equation	Spatial Resolution (m)	Reference
Chlorophyll Absorption Ratio Index	CARI	$\left(\frac{RED\ EDGE\ 5}{RED}\right)\frac{\sqrt{(a.RED+RED+b)^2}}{(a^2+1)^{0.5}}$ α = (RED EDGE 5 − GREEN)/150 b = (GREEN − ((RED EDGE 5 − GREEN)/150, 550))	20	[34]
Enhanced Vegetation Index	EVI	$2.5\frac{NIR-RED}{(NIR+6RED+7.5BLUE)+1}$	10	[35]
Green Normalized Difference Vegetation Index	GNDVI	$\frac{NIR-GREEN}{NIR+GREEN}$	10	[36]
Modified Simple Ratio	MSR	$\frac{\frac{NIR}{RED}-1}{\sqrt{\frac{NIR}{RED}+1}}$	10	[37]
Modified Triangular Vegetation Index 1	MTVI1	$1.2\,[1.2\,(NIR-GREEN)-2.5\,(RED-GREEN)]$	10	[38]
Normalized Difference Vegetation Index	NDVI	$\frac{(NIR-RED\ EDGE\ 5)}{(NIR+RED\ EDGE\ 5)}$	10	[39]
Soil Adjusted Vegetation Index	SAVI	$\frac{NIR-RED}{NIR+RED+0.5}\cdot(1+0.5)$	10	[40]

2.3. Must Quality Data

A reference dataset which included the analyses of soluble solids (° Brix), total acidity (g/L) and pH measured at harvest by Fourier Transform Infrared (FITR) with Oenofoss (FOSS. Electric, Hillerød, Denmark) for 2017, 2018, and 2019 was available.

The 2017 dataset included 50 samples from F and 70 from NF. A total amount of 226 samples (103 from F and 123 NF) and 193 samples (89 from F and 104 from NF) were selected for 2018 and 2019, respectively.

The properties of must quality recorded at harvest for F and NF plots were used as a proxy to assess if the growth observed using satellite imagery lead to significant differences in grape maturation.

2.4. Statistical Analyses

First, the reflectance of every single pixel of the 2017 images was normalized by dividing each value by the average reflectance of 2018 and 2019. Images from corresponding dates in 2018 and 2019 were used for this purpose. Due to protracted cloud cover, in 2018 and 2019 images for the 24th of May or close dates were not available. To overcome this problem, linear interpolation was performed between the values of VIs and spectral band before and after the missing date for both years [41]. The normalization aimed to minimize the influence of interannual differences in weather and vegetation conditions [42]. The interannual normalization ($inVI_{i,Sk}$) for the i-th pixel and for the Sk-th date is shown in Equation (1).

$$inVI_{i,\ Sk} = \frac{VI_{i,Sk,2017}}{\frac{1}{2n}\left(\sum_{i=1}^{n} VI_{i,Sk,2018} + \sum_{i=1}^{n} VI_{i,Sk,2019}\right)} \quad (1)$$

where n is the total number of pixels of acquired images, $VI_{i,Sk,2017}$, $VI_{i,Sk,2018}$, $VI_{i,Sk,2019}$ represent the reflectance value of the i-th pixel for the considered VI/spectral band at the Sk-th date in 2017, 2018, and 2019 respectively. Next, the normalized values of 2017 were implemented in order to calculate VIs, which were once more normalized to the first available date (S1), equating to 1. Therefore, normalized values < 1 indicate lower reflectance compared to S1, whereas values > 1 indicate higher reflectance. Since the spectral reflectance that can be captured by satellite images is affected by the contribution from different factors, further normalization helped to avoid the influence of environmental factors that were not of interest in the present study. The normalized values of the VIs, referred to henceforth as nVIs [42], for the i-th pixel and the Sk-th date, were computed by means of Equations (2) and (3).

$$nVI_{i,Sk} = \frac{inVI_{i,Sk}}{\frac{1}{n}\sum_{i=1}^{n} inVI_{i,S1}} \quad (2)$$

$$nVI(Sk) = \frac{1}{n}\sum_{i=1}^{n} nVI_{i,Sk} \quad (3)$$

where Sk indicates S2, S3, S4 and S5 (Table 2). NVI values in the different dates were finally compared using a Student unpaired, t-test with R statistical software with the level of significance (p) based on the degree of freedom (df) and t-statistic (t): * $p < 0.05$, ** $p < 0.01$, *** $p < 0.001$. The test allowed for the detection of significative mean differences between NF and F, establishing the effect of the frost event and assessing the recovery time.

The normalization of spectral reflectance to minimize different sources of remote sensing measurement error has been used by several authors [42–46]. These authors proposed different approaches for the interannual normalization of NDVI. The method used in the current study aimed at: (i) minimizing the interannual differences (1), (ii) comparing time-series data (2).

Similarly, the must quality data for 2017 were normalized on the average for each parameter (soluble solids, total acidity and pH) of the 2018 and 2019 both for F (Equations (4)–(6)).

$$nSS = \frac{\sum_{j=1}^{50} SS_{j,2017}}{\frac{1}{192}\left(\sum_{j=1}^{103} SS_{j,2018} + \sum_{j=1}^{89} SS_{j,2019}\right)} \quad (4)$$

$$nTA = \frac{\sum_{j=1}^{50} TA_{j,2017}}{\frac{1}{192}\left(\sum_{j=1}^{103} TA_{j,2018} + \sum_{j=1}^{89} TA_{j,2019}\right)} \quad (5)$$

$$npH = \frac{\sum_{j=1}^{50} pH_{j,2017}}{\frac{1}{192}\left(\sum_{j=1}^{103} pH_{j,2018} + \sum_{j=1}^{89} pH_{j,2019}\right)} \quad (6)$$

and NF (Equations (7)–(9)):

$$nSS = \frac{\sum_{j=1}^{70} SS_{j,2017}}{\frac{1}{227}\left(\sum_{j=1}^{123} SS_{j,2018} + \sum_{j=1}^{104} SS_{j,2019}\right)} \quad (7)$$

$$nTA = \frac{\sum_{j=1}^{70} TA_{j,2017}}{\frac{1}{227}\left(\sum_{j=1}^{123} TA_{j,2018} + \sum_{j=1}^{104} TA_{j,2019}\right)} \quad (8)$$

$$npH = \frac{\sum_{i=1}^{70} pH_{j,2017}}{\frac{1}{227}\left(\sum_{j=1}^{123} pH_{j,2018} + \sum_{j=1}^{104} pH_{j,2019}\right)} \quad (9)$$

where $TA_{j,year}$, $SS_{j,year}$ and $pH_{j,year}$ represent total acidity, soluble solids and pH for the j-th available sample for 2017, 2018, or 2019. The normalized values of F and NF were compared with a Student unpaired, t-test using GraphPad Prism 8.0.0 (GraphPad Software, Inc.; La Jolla, CA, USA).

3. Results

3.1. Vegetation Indices

Most of the VIs were able to detect the frost damage and, to a greater extent, the recovery of the injured vines. nCARI, nMTVI1 and nEVI decreased significantly after the frost event (Figure 4). Specifically, nCARI displayed significant difference on the 24th of May (t = −9.847, df = 114). nMTVI1 highlighted significant difference on the 14th of May (t = −1.346, df = 450) and nEVI on the 24th of May (t = 50.692, df = 618), with −16.59% relative reflectance in F compared to NF. nCARI, nMTVI1 and nEVI allowed to identify significant recovery after the 24th of May (June 3: t = 10.828, df = 184; t = 25.95, df = 495; t = 28.326, df = 482; June 23: t = 50.692, df = 618; t = 47.005, df = 517; t = 5.285, df = 126, respectively). nNDVI did not exhibit significant difference between F and NF (Figure 5) after the frost event but, consistently with the other VIs indicated vine recovery after the 24th of May (June 3: t = 33.402, df = 501; June 23: t = 38.588, df = 658).

nMSR increased significantly after the frost event (May 14: t = 73.193, df = 465), dropped on the 24th of May, and then increased again after this date (June 3: t = 7.295, df = 575; June 23: t = 18.877, df = 670). nGNDVI failed to provide valuable results, exhibiting a better performance in F during all the observed period. Figure 5 shows the nNDVI and nMSR time-series.

Table 5 reports the values of the relative reflectance differences in F compared to NF for the nVIs on the different dates.

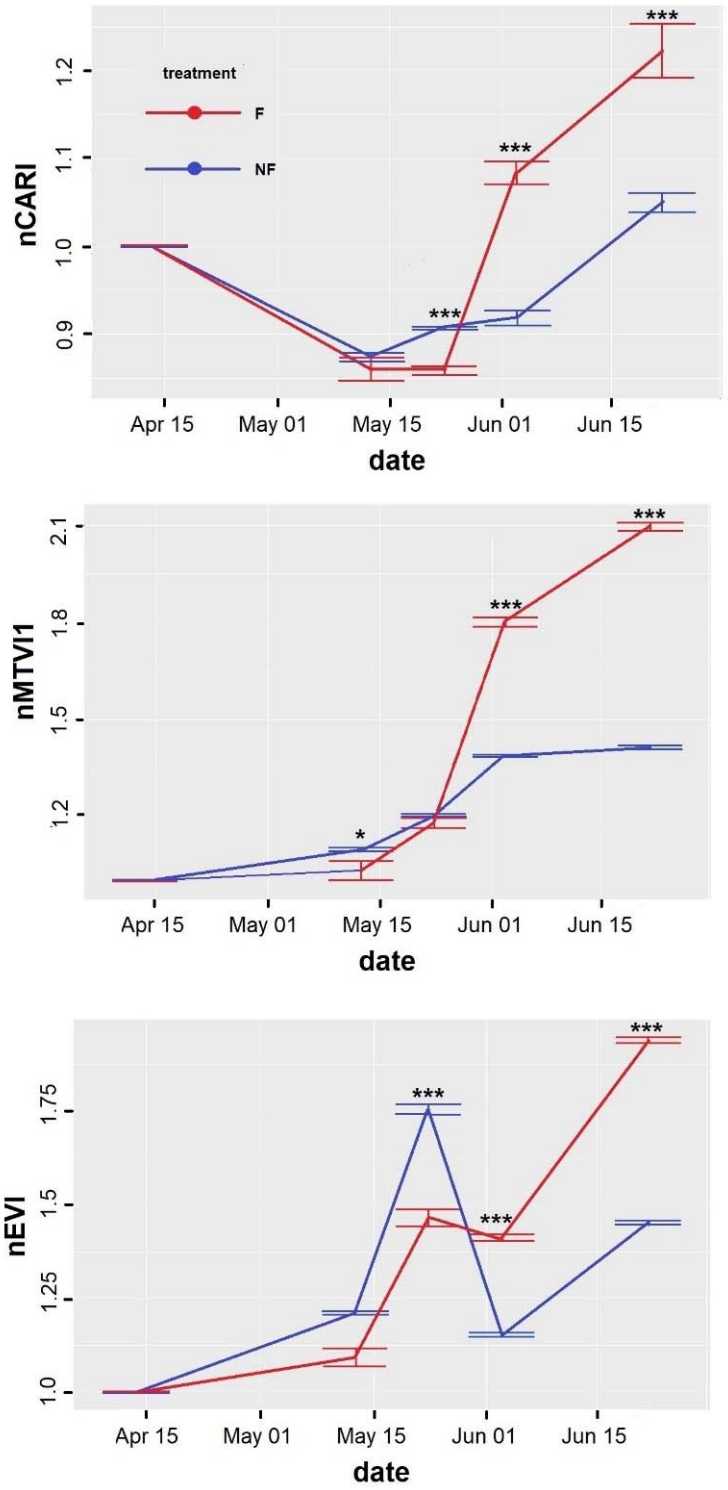

Figure 4. Change of normalized CARI, MTVI1, and EVI from May to June 2017. The values reported in y axis represent the reflectance values normalized on the first date, equating to 1. Statistical significance was determined by Student's *t*-test. Single asterisk indicates a significant difference between treatments, $p < 0.05$; double asterisk indicates a statistical difference, $p < 0.01$; triple asterisk indicates a statistical difference, $p < 0.001$ (unpaired *t*-test). Error bars represent standard error of the mean.

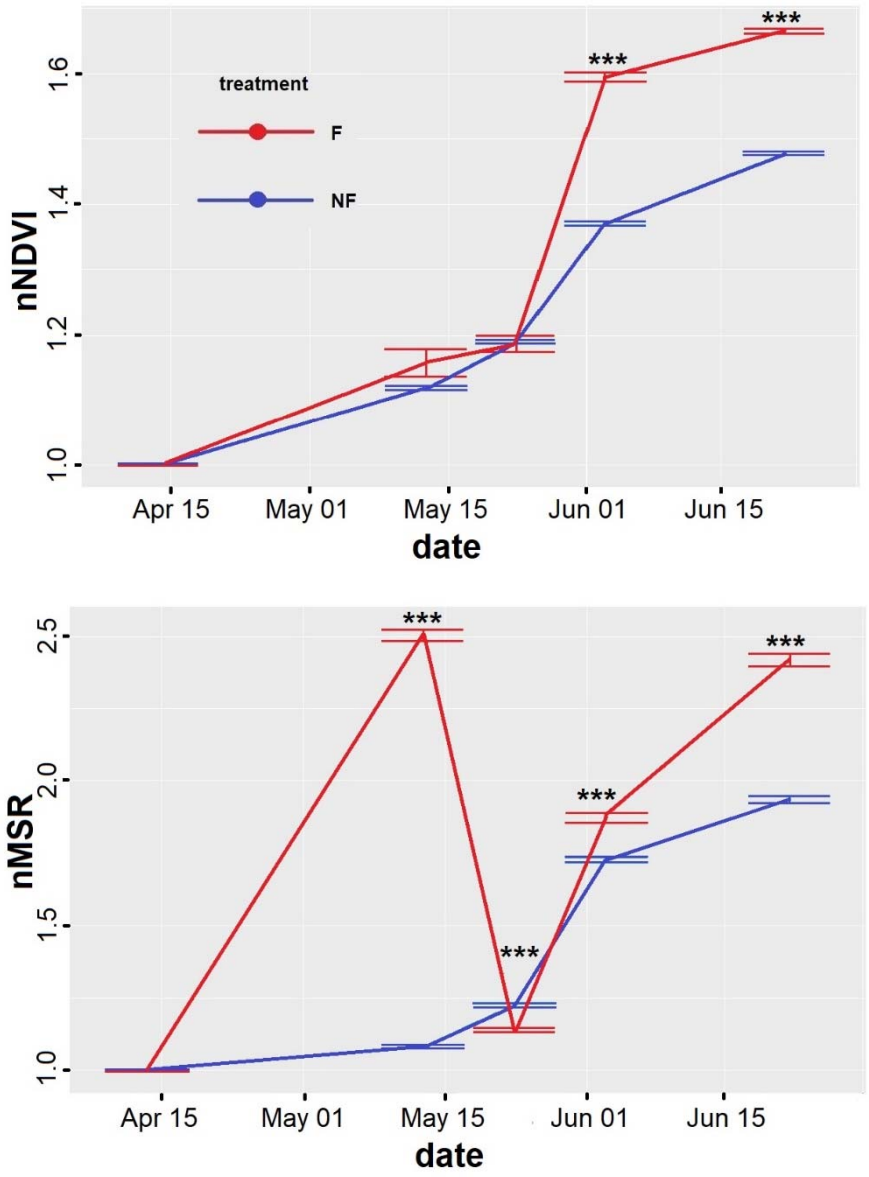

Figure 5. Change of normalized NDVI and MSR from May to June 2017. The values reported in y axis represent the reflectance values normalized on the first date, equating to 1. Statistical significance was determined by Student's *t*-test. Single asterisk indicates a significant difference between treatments, $p < 0.05$; double asterisk indicates a statistical difference, $p < 0.01$; triple asterisk indicates a statistical difference, $p < 0.001$ (unpaired *t*-test). Error bars represent standard error of the mean.

Table 5. Differences in the relative reflectance of the nVIs computed in F compared to NF. Single asterisk indicates a significant difference, $p < 0.05$; double asterisk indicates a statistical difference, $p < 0.01$; triple asterisk indicates a statistical difference, $p < 0.001$ (unpaired *t*-test); ns indicates not significant difference ($p > 0.05$).

VI	Difference (%)			
	14/05/2017	**24/05/2017**	**03/06/2017**	**23/06/2017**
nCARI	−1.74 (ns)	−5.26 (***)	+17.70 (***)	+16.41 (***)
nEVI	−9.77 (ns)	−16.29 (***)	+22.42 (***)	+33.43 (***)
nMSR	+130.73 (***)	−7.36 (***)	+8.73 (***)	+24.80 (***)
nMTVI1	−5.77 (*)	−1.91 (ns)	+29.67 (***)	+48.03 (***)
nNDVI	+3.49 (ns)	−0.33 (ns)	+16.48 (***)	+12.72 (***)

3.2. Spectral Bands

The nNIR and the nRed Edge (Sentinel-2 band 7) spectral bands showed significant differences between F and NF after the frost event. The reflectance in the nNIR band dropped after the 17th of April showing highly significant difference both on the 14th of May (t = −12.365, df = 494) and the 24th of May (t = −36.051, df = 475). After this date, the nNIR reflectance increased sharply in F, compared to NF (June 3: t = 9.924, df = 521; June 23: t = 28.196, df = 611). The trend of nRed Edge 7 was very similar (14 May: t = −7.310, df = 119; May 24: t = −5.958, df = 111; June 3: t = 5.409, df = 140; June 23: t = 13.746, df = 138). The performance of nRed Edge 5 and nRed Edge 6 were not as satisfactory as the one of nRed Edge 7 (data not shown), with nRed Edge 6 showing significant difference only on 24th of May and 23rd of June and nRed Edge 5 exhibiting lower values for F across all the season, except for the 23rd of June. The nSWIR did not detect the effect of frost event on vines (data not shown). Figure 6 shows the nNIR and nRed Edge 7 time-series. Table 6 reports the values of the relative reflectance differences in F compared to NF for the normalized spectral bands on the different dates.

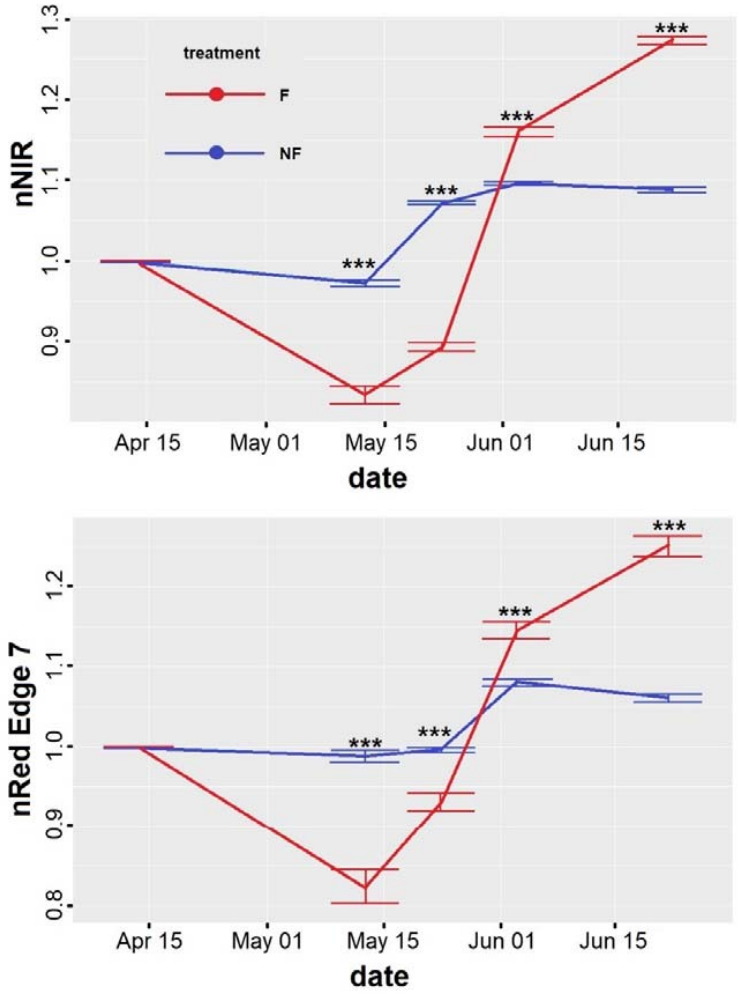

Figure 6. Change of normalized NIR and Red Edge (Sentinel-2 band 7) from May to June 2017. The values reported in y axis represent the reflectance values normalized on the first date, equating to 1. Statistical significance was determined by Student's *t*-test. Single asterisk indicates a statistical difference between treatments, $p < 0.05$; double asterisk indicates a significant difference, $p < 0.01$; triple asterisk indicates a statistical difference, $p < 0.001$ (unpaired *t*-test). Error bars represent standard error of the mean.

Table 6. Differences in the relative reflectance of the normalized spectral bands computed in F compared to NF. Single asterisk indicates a significant difference, $p < 0.05$; double asterisk indicates a statistical difference, $p < 0.01$; triple asterisk indicates a statistical difference, $p < 0.001$ (unpaired *t*-test).

Spectral Band	Difference (%)			
	14/05/2015	**24/05/2017**	**03/06/2017**	**23/06/2017**
nNIR	−14.33 (***)	−16.65 (***)	+5.89 (***)	+17.04 (***)
nRed Edge 7	−16.67 (ns)	−6.53 (***)	+5.91 (***)	+17.90 (***)

3.3. Must Quality Data

As harvest time was decided on the basis of the sugar content of the grapes, no significant differences were observed among F and NF plots, even if the former were harvested between the 11th and the 23rd of September, and the latter between the 22nd of August and the 4th of October. On the contrary, highly significant differences were found in 2017 among F and NF for total acidity and pH (Figure 7) which may be in response to the late frost. Specifically, total acidity was higher ($p = 0.015$), and pH was lower ($p < 0.0001$) in F compared to NF due to the shorter vegetative season. As for the spectral data, the normalized values of the must parameters are reported in Figure 7.

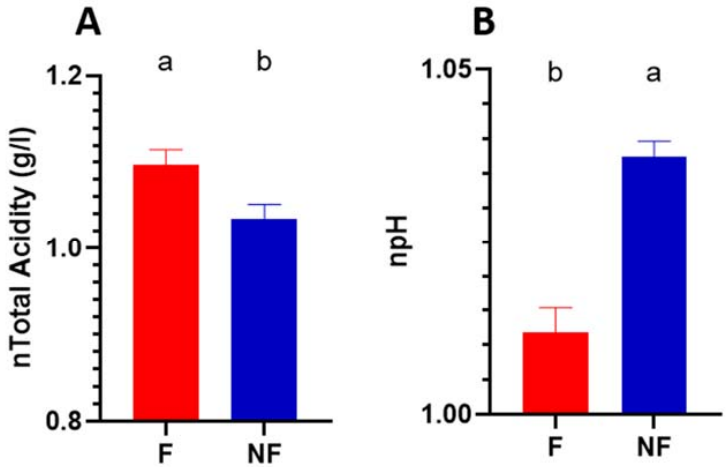

Figure 7. Normalized values of total acidity (**A**) and pH (**B**) recorded at harvest. Values represent the mean ± SE for F ($n = 50$) and NF ($n = 70$). Values were normalized on the average of 2018–2019. Different letters indicate significant differences among treatments according to Student's *t*-test ($p \leq 0.05$).

4. Discussion

In this study, the effectiveness of remotely sensed spectral data to detect damage caused by frost events was tested, as well as the recovery time of frost-affected vines.

The findings were limited by the availability of remote sensing data. After the late frost event, the weather conditions were adverse, with almost complete cloud coverage. As a result, the first spectral data were available one month after the frost event. Nevertheless, the results showed that remote-sensed VIs detected frost damage and were able to capture the vineyard recovery over time.

The VIs that provided the best description of the changes of the vegetation after a late frost were nCARI, nMTVI1 and nEVI (Figure 4).

The MTVI1 is a VI sensitive to changes in leaf and canopy structure [38,47], which was formulated to minimize the sensitiveness to soil background of the Triangular Vegetation Index (TVI). After the frost event, the damaged shoots were replaced by the development of secondary buds. On 14th of May, after the frost event, the performance of MTVI1 in F was significantly different from NF. The lower value of MTVI1 was likely due to the underdevelopment of the new shoots in F after the frost event. Starting from the following available date (3 June), the values of nMTVI1 in F younger

shoots were higher, indicating that full recovery may have occurred between the 24th of May and the 3rd of June, as confirmed by the winegrowers' cooperative. In a study on frost damage in oilseed rape (*Brassica Napus* L.) using a VIS/NIR imaging spectrophotometer, Duddu et al. [22] achieved similar results using TVI.

EVI is another structural VI, sensitive to LAI and canopy biomass and less reactive to canopy background signals [48], which was used on previous studies on late frost [18,49]. The trend of nEVI during the observed period shows a peak both in F and NF corresponding to the flowering phenological stage. The decline after this stage is expected [50], although it should keep on decreasing till harvest. It should be noted that in both the F and NF study areas, even if cover crops in the interrow was mowed regularly, it might have partially contributed to the measured reflectance, especially in the early phenological stages [51,52]. Despite the contribution of cover crops to the spectral reflectance is negligible only after veraison in Vertical Shoot Positioned (VSP) trellis systems [53,54], it is worth highlighting that with horizontal roof training systems (such as "Pergola" in the present study) and with early growth varieties (such as Garganega in the present study) a low influence of the interrow was assessed already at flowering.

In this study, nNDVI values of F were not significantly different from NF after the frost event (Figure 5). Previous studies on annual crops identified NDVI as a valuable indicator of frost damage. Feng et al. [55] observed a dramatic drop of NDVI derived using multi-temporal MODIS imagery in winter wheat and similar results were found using Huanjing satellite (HJ) images [56]. She et al. [18] estimated a 53.7% decrease of NDVI values after a cold spell in oilseed rape. In contrast with these studies, Duddu et al. [22] detected an increase of NDVI in frost-affected oilseed rape, asserting that the reason might be related to the lower reflectance in the red region caused by the discoloration of leaves to dark green. In the current analysis, nNDVI was only effective at providing information on the recovery time. In early-season images, cover crops may have a strong influence on the NDVI response [53], and this is probably the reason this VI failed to detect frost damage in this study. For the same reason, nMSR was only effective for the assessment of the recovery time. nMSR showed a drastic increase of the signal in F area between the 14th of April and the 14th of May, followed by a sudden reduction on the 3rd of June (Figure 5). With respect to the nNDVI index such variation was likely more evident due to the quadratic rate between numerator and denominator in the MSR equation.

A final comment on the results of the VIs used in this study is that three-band VIs (CARI, MTVI1, EVI) performed better than two-band ones. Three-band indices where developed to address the saturation issue [57] and this make them more sensitive in detecting the structural and chlorophyll changes in frost-affected grapevines.

The spectral bands which provided better results were the NIR and the Red Edge (band 7) (Figure 6). These spectral bands are commonly associated with different crop stresses, such as drought [58–60], heatwaves [24], frost [22,61] and nitrogen deficiency [62]. The Red Edge is an indicator of the chlorophyll concentration and LAI, which are very likely affected by late frost events. The reduced reflectance in the NIR region after frost is probably due to the combination of changes in pigment concentration [61] and water content [22] at the cellular level.

When dealing with grapevine, the main limitation posed using medium-resolution spectral information is the mixed nature of pixels. The pixel-spacing of 10 × 10 or 20 × 20 m implies the inclusion of both rows and inter-rows, affecting crop status evaluation [52]. This spatial resolution limits the employment of Sentinel-2 imagery to areas larger than 0.5 ha [26,33]. Moreover, the cloud coverage may represent a limitation to the usability of the images, especially during early spring, when weather conditions are unstable. On the other hand, the use of high-resolution imagery might become extremely expensive and challenging in some situations. Medium-resolution data may be the most cost-effective to inspect large areas, particularly in the case of extreme weather events. Previous studies provided evidence of the agreement between VIs calculated from high- and medium-resolution images and the feasibility to use Sentinel-2 spectral data to obtain valuable information on vineyards [24–26]. Therefore, while we are aware that using higher-resolution products would improve the results, the findings of

this study highlighted that Sentinel-2 data could support decision-making towards assessment and recovery management.

The analysis of the must quality data recorded at harvest was used as a side quantification to assess any maturity changes related to the 2017 late frost experienced by the F vineyards. Recent research on the effect of late frost on berry composition is lacking. A significant increase in total acidity was observed in the must from frost-affected *Vitis vinifera* cv. Tokay, Carignane and Zinfandel [63]. The same study did not detect any significant difference in sugar concentration as similarly to the present study, harvest time was decided when a specific sugar content was achieved. On the contrary, other studies did not find difference in the parameters characterizing the commercial maturity [64]. Regardless of the conclusions of the mentioned studies, the influence of temperature on acidity and pH is well known [65,66]. The results shown in Figure 7 suggest that in 2017, the delayed phenology caused by the frost damage to the buds had likely induced higher acidity and lower pH in F [67]. The shorter ripening period of F grapes reduced the time for losses in acidity, altering composition at harvest. It must be underlined that due to the reduced number of must quality parameters of the dataset, these results should be supported by further data and analysis.

5. Conclusions

The present study investigated for the first time the effectiveness of medium-spatial resolution imagery from Sentinel-2 Mission to detect the damage in late frost-affected vineyards. Furthermore, VIs and spectral bands were tested for their potential to assess the recovery time. The traditional damage assessment methods are labor-intensive, costly, and usually conducted within small areas. Therefore, these methods do not represent the best option to manage these events at a regional level. This study aimed to investigate an efficient and cost-effective conceptual methodology for assessing a late frost event and recovery time detection. The frequent revisit time of Sentinel-2 constellation allows for the generation of a robust time-series for spatio-temporal analyses. Thus, this approach might be used not only for damage assessment but also for the continuous monitoring of the status of the vines after frost events. The results showed for the first time that the spectral reflectance from medium-resolution imagery is responsive to frost damage. In detail, the specific spectral regions and VIs which were capable of detecting the frost damage, showing lower reflectance, were Red Edge 7 (−16.67), NIR (−16.55%), EVI (−16.59%), MTVI1 (−5.77%) and CARI (−5.26%), The same VIs/spectral bands provided evidence of full recovery of the vines 40 days after the frost event. NDVI and MSR, which were not reactive to frost damage, gave further proof of the recovery time. The findings were consistent with other studies on annual crops. Achieving valuable information from open-access imagery represents a step forward in the frost management from local to global scale. The chance of missing data, due to cloud cover, could be a limiting factor but the frequency of capture increases the opportunity to obtain sufficient information. Further investigation will be needed, on different varieties, areas, and training system, to confirm the findings of this study. Nevertheless, the results provide evidence that the methods implemented can provide useful information to assess the impact of late frost on grapevines.

Author Contributions: Conceptualization, A.C., F.M. (Francesco Marinello), F.M. (Franco Meggio); collecting data and research methodology, A.C., F.M. (Francesco Marinello); validation and formal analysis, A.C., F.M. (Francesco Marinello), F.M. (Franco Meggio), C.C.; writing—original draft preparation, A.C.; writing—review, A.C., F.M. (Francesco Marinello), F.M. (Franco Meggio), C.C.; supervision, F.M. (Francesco Marinello). All authors have read and agreed to the published version of the manuscript.

Funding: This research was funded by Italian Ministry of Research and University (MIUR) in the frame of SIR 2014, grant number RBSI14H5R0.

Acknowledgments: The authors would like to thank Collis Veneto wine Group for providing information on the sample areas.

Conflicts of Interest: The authors declare no conflict of interest.

References

1. Meier, M.; Fuhrer, J.; Holzkämper, A. Changing risk of spring frost damage in grapevines due to climate change? A case study in the Swiss Rhone Valley. *Int. J. Biometeorol.* **2018**, *62*, 991–1002. [CrossRef]
2. Lisek, J. Climatic factors affecting development and yielding of grapevine in Central Poland. *J. Fruit Ornam. Plant Res.* **2008**, *16*, 285–293.
3. Leolini, L.; Moriondo, M.; Fila, G.; Costafreda-Aumedes, S.; Ferrise, R.; Bindi, M. Late spring frost impacts on future grapevine distribution in Europe. *Field Crop. Res.* **2018**, *222*, 197–208. [CrossRef]
4. Crimp, S.J.; Zheng, B.; Khimashia, N.; Gobbett, D.L.; Chapman, S.; Howden, M.; Nicholls, N. Recent changes in southern Australian frost occurrence: Implications for wheat production risk. *Crop Pasture Sci.* **2016**, *67*, 801–811. [CrossRef]
5. Molitor, D.; Caffarra, A.; Sinigoj, P.; Pertot, I.; Hoffmann, L.; Junk, J. Late frost damage risk for viticulture under future climate conditions: A case study for the Luxembourgish winegrowing region. *Aust. J. Grape Wine Res.* **2014**, *20*, 160–168. [CrossRef]
6. Sgubin, G.; Swingedouw, D.; Dayon, G.; García de Cortázar-Atauri, I.; Ollat, N.; Pagé, C.; van Leeuwen, C. The risk of tardive frost damage in French vineyards in a changing climate. *Agric. For. Meteorol.* **2018**, *250–251*, 226–242. [CrossRef]
7. Mosedale, J.R.; Wilson, R.J.; Maclean, I.M.D. Climate change and crop exposure to adverse weather: Changes to frost risk and grapevine flowering conditions. *PLoS ONE* **2015**, *10*, e0141218. [CrossRef] [PubMed]
8. Johnson, D.E.; Howell, G.S. Factors Influencing Critical Temperatures for Spring Freeze Damage to Developing Primary Shoots on Concord Grapevines. *Am. J. Enol. Vitic.* **1981**, *32*, 144–149.
9. Trought, M.C.T.; Bennett, J.S.; Boldingh, H.L. Influence of retained cane number and pruning time on grapevine yield components, fruit composition and vine phenology of Sauvignon Blanc vines. *Aust. J. Grape Wine Res.* **2011**, *17*, 258–262. [CrossRef]
10. Fuller, M.P.; Telli, G. An investigation of the frost hardiness of grapevine (*Vitis vinifera*) during bud break. *Ann. Appl. Biol.* **1999**, *135*, 589–595. [CrossRef]
11. Poling, E.B. Spring cold injury to winegrapes and protection strategies and methods. *HortScience* **2008**, *43*, 1652–1662. [CrossRef]
12. Dami, I. Freezing and Survival Mechanisms of Grapevines. In Proceedings of the Understanding and Preventing Freeze Damage in Vineyards Workshop, Columbia, MO, USA, 5–6 December 2007; pp. 13–20.
13. Ishikawa, M.; Ide, H.; Yamazaki, H.; Murakawa, H.; Kuchitsu, K.; Price, W.S.; Arata, Y. Freezing behaviours in wintering *Cornus florida* flower bud tissues revisited using MRI. *Plant Cell Environ.* **2016**, *39*, 2663–2675. [CrossRef] [PubMed]
14. Wisniewski, M.; Gusta, L.; Neuner, G. Adaptive mechanisms of freeze avoidance in plants: A brief update. *Environ. Exp. Bot.* **2014**, *99*, 133–140. [CrossRef]
15. De Leeuw, J.; Vrieling, A.; Shee, A.; Atzberger, C.; Hadgu, K.M.; Biradar, C.M.; Keah, H.; Turvey, C. The potential and uptake of remote sensing in insurance: A review. *Remote Sens.* **2014**, *6*, 10888–10912. [CrossRef]
16. Black, E.; Greatrex, H.; Young, M.; Maidment, R. Incorporating satellite data into weather index insurance. *Bull. Am. Meteorol. Soc.* **2016**, *97*, ES203–ES206. [CrossRef]
17. Bokusheva, R.; Kogan, F.; Vitkovskaya, I.; Conradt, S.; Batyrbayeva, M. Satellite-based vegetation health indices as a criteria for insuring against drought-related yield losses. *Agric. For. Meteorol.* **2016**, *220*, 200–206. [CrossRef]
18. She, B.; Huang, J.F.; Guo, R.F.; Wang, H.B.; Wang, J. Assessing winter oilseed rape freeze injury based on Chinese HJ remote sensing data. *J. Zhejiang Univ. Sci. B* **2015**, *16*, 131–144. [CrossRef]
19. She, B.; Huang, J.F.; Zhang, D.Y.; Huang, L.S. Assessing and characterizing oilseed rape freezing injury based on MODIS and MERIS data. *Int. J. Agric. Biol. Eng.* **2017**, *10*, 143–157.
20. Currit, N.; St Clair, S.B. Assessing the impact of extreme climatic events on aspen defoliation using modis imagery. *Geocarto Int.* **2010**, *25*, 133–147. [CrossRef]
21. LI, Z.-C.; Zhou, Q.-B.; Lu, X.; Lin, H.-R.; Li, S. Hyperspectral Features of Winter Wheat after Frost Stress at Jointing Stage. *Acta Agron. Sin.* **2008**, *34*, 831–837. [CrossRef]
22. Duddu, H.S.N.; Pajic, V.; Noble, S.D.; Tanino, K.K.; Shirtliffe, S.J. Image-Based Rapid Estimation of Frost Damage in Canola (*Brassica napus* L.). *Can. J. Remote Sens.* **2018**, *44*, 169–175. [CrossRef]

23. Su, B.F.; Xue, J.R.; Xie, C.Y.; Fang, Y.L.; Song, Y.Y.; Fuentes, S. Digital surface model applied to unmanned aerial vehicle based photogrammetry to assess potential biotic or abiotic effects on grapevine canopies. *Int. J. Agric. Biol. Eng.* **2016**, *9*, 119–130.
24. Cogato, A.; Pagay, V.; Marinello, F.; Meggio, F.; Grace, P.; De Antoni Migliorati, M. Assessing the feasibility of using medium-resolution imagery information to quantify the impact of the heatwaves on irrigated vineyards. *Remote Sens.* **2019**, *11*, 2869. [CrossRef]
25. Borgogno-Mondino, E.; Lessio, A.; Tarricone, L.; Novello, V.; de Palma, L. A comparison between multispectral aerial and satellite imagery in precision viticulture. *Precis. Agric.* **2018**, *19*, 195–217. [CrossRef]
26. Sozzi, M.; Kayad, A.; Marinello, F.; Taylor, J.; Tisseyre, B. Comparing vineyard imagery acquired from Sentinel-2 and Unmanned Aerial Vehicle (UAV) platform. *OENO One* **2020**, *54*, 189–197. [CrossRef]
27. Di Gennaro, S.F.; Dainelli, R.; Palliotti, A.; Toscano, P.; Matese, A. Sentinel-2 validation for spatial variability assessment in overhead trellis system viticulture versus UAV and agronomic data. *Remote Sens.* **2019**, *11*, 2573. [CrossRef]
28. Sun, L.; Gao, F.; Anderson, M.C.; Kustas, W.P.; Alsina, M.M.; Sanchez, L.; Sams, B.; McKee, L.; Dulaney, W.; White, W.A.; et al. Daily mapping of 30 m LAI and NDVI for grape yield prediction in California vineyards. *Remote Sens.* **2017**, *9*, 317. [CrossRef]
29. Ciraolo, G.; Capodici, F.; D'Urso, G.; La Loggia, G.; Maltese, A. Mapping evapotranspiration on vineyards: The Sentinel-2 potentiality. In Proceedings of the Sentinel-2 Preparatory Symposium, Frascati, Italy, 23–27 April 2012; p. 707.
30. Cunha, M.; Marçal, A.R.S.; Silva, L. Very early prediction of wine yield based on satellite data from vegetation. *Int. J. Remote Sens.* **2010**, *31*, 3125–3142. [CrossRef]
31. Hack, H.; Bleiholder, H.; Buhr, L.; Meier, U.; Schnock-Fricke, U.; Weber, E.; Witzenberger, A. Einheitliche Codierung der phänologischen Entwicklungsstadien mono- und dikotyledoner Pflanzen. Erweitere BBCH-Skala, Allgemeine. *Nachrichtenbl. Deut. Pflanzenschutzd* **1992**, *44*, 270.
32. Louis, J.; Debaecker, V.; Pflug, B.; Main-Knorn, M.; Bieniarz, J.; Mueller-Wilm, U.; Cadau, E.; Gascon, F. Sentinel-2 SEN2COR: L2A processor for users. In Proceedings of the ESA Living Planet Symposium 2016, Prague, Czech Republic, 9–13 May 2016; pp. 9–13.
33. Devaux, N.; Crestey, T.; Leroux, C.; Tisseyre, B. Potential of Sentinel-2 satellite images to monitor vine fields grown at a territorial scale. *OENO One* **2019**, *53*, 51–58. [CrossRef]
34. Kim, M.S.; Daughtry, C.S.T.; Chappelle, E.W.; McMurtrey, J.E. The use of high spectral resolution bands for estimating absorbed photosynthetically active radiation (APAR). In Proceedings of the ISPRS 94, Val d'Isere, France, 17–21 January 1994; pp. 299–306.
35. Huete, A.; Justice, C.; Van Leeuwen, W. *MODIS Vegetation Index (MOD 13)*; Algorithm Theoretical Basis Document, Version 3; University of Arizona: Tucson, AZ, USA; University of Virginia: Charlotteville, VA, USA, 1999.
36. Gitelson, A.A.; Merzlyak, M.N. Remote sensing of chlorophyll concentration in higher plant leaves. *Adv. Sp. Res.* **1998**, *22*, 689–692. [CrossRef]
37. Chen, J.M. Evaluation of vegetation indices and a modified simple ratio for boreal applications. *Can. J. Remote Sens.* **1996**, *22*, 229–242. [CrossRef]
38. Haboudane, D.; Miller, J.R.; Pattey, E.; Zarco-Tejada, P.J.; Strachan, I.B. Hyperspectral vegetation indices and novel algorithms for predicting green LAI of crop canopies: Modeling and validation in the context of precision agriculture. *Remote Sens. Environ.* **2004**, *90*, 337–352. [CrossRef]
39. Rouse, J.; Haas, R.; Schell, J.; Deering, D.; Harlan, J. *Monitoring the Vernal Advancement and Retrogradation (Greenwave Effect) of Natural Vegetation*; NASA: Washington, DC, USA, 1974.
40. Baret, F.; Guyot, G. Potentials and limits of vegetation indices for LAI and APAR assessment. *Remote Sens. Environ.* **1991**, *35*, 161–173. [CrossRef]
41. Schmidt, T.; Förster, M.; Kleinschmit, B. Evaluation of estimated satellite images for filling data gaps in an intra-annual high spatial resolution time-series. In *Accuracy 2014, Proceedings of the 11th International Symposium on Spatial Accuracy Assessment in Natural Resources and Environmental Sciences, East Lansing, MI, USA, 8–11 July 2014*; ISARA: Catania, Italy, 2014; pp. 2–7.
42. VandeKamp, K.; Rigge, M.; Troelstrup, N.H.; Smart, A.J.; Wylie, B. Detecting channel riparian vegetation response to best-management-practices implementation in ephemeral streams with the use of spot high-resolution visible imagery. *Rangel. Ecol. Manag.* **2013**, *66*, 63–70. [CrossRef]

43. Kogan, F.N. Remote sensing of weather impacts on vegetation in non-homogeneous areas. *Int. J. Remote Sens.* **1990**, *11*, 1405–1419. [CrossRef]
44. Liang, L.; Sun, Q.; Luo, X.; Wang, J.; Zhang, L.; Deng, M.; Di, L.; Liu, Z. Long-term spatial and temporal variations of vegetative drought based on vegetation condition index in China. *Ecosphere* **2017**, *8*, e01919. [CrossRef]
45. Choler, P.; Sea, W.; Leuning, R. A Benchmark Test for Ecohydrological Models of Interannual Variability of NDVI in Semi-arid Tropical Grasslands. *Ecosystems* **2011**, *14*, 183–197. [CrossRef]
46. Potdar, M.B.; Manjunath, K.R.; Purohit, N.L. Multi-season atmospheric normalization of NOAA AVHRR derived NDVI for crop yield modeling. *Geocarto Int.* **1999**, *14*, 52–57. [CrossRef]
47. Zarco-Tejada, P.J.; Ustin, S.L.; Whiting, M.L. Temporal and spatial relationships between within-field yield variability in cotton and high-spatial hyperspectral remote sensing imagery. *Agron. J.* **2005**, *97*, 641–653. [CrossRef]
48. Gao, X.; Huete, A.R.; Ni, W.; Miura, T. Optical-biophysical relationships of vegetation spectra without background contamination. *Remote Sens. Environ.* **2000**, *74*, 609–620. [CrossRef]
49. Bascietto, M.; Bajocco, S.; Ferrara, C.; Alivernini, A.; Santangelo, E. Estimating late spring frost-induced growth anomalies in European beech forests in Italy. *Int. J. Biometeorol.* **2019**, *63*, 1039–1049. [CrossRef] [PubMed]
50. Fraga, H.; Amraoui, M.; Malheiro, A.C.; Moutinho-Pereira, J.; Eiras-Dias, J.; Silvestre, J.; Santos, J.A. Examining the relationship between the Enhanced Vegetation Index and grapevine phenology. *Eur. J. Remote Sens.* **2014**, *47*, 753–771. [CrossRef]
51. Marciniak, M. Use of remote sensing to understand the terroir of the Niagara Peninsula. Applications in a Riesling vineyard. *J. Int. Sci. Vigne Vin* **2015**, *49*, 1–26. [CrossRef]
52. Khaliq, A.; Comba, L.; Biglia, A.; Aimonino, D.R.; Chiaberge, M.; Gay, P. Comparison of satellite and UAV-based multispectral imagery for vineyard variability assessment. *Remote Sens.* **2019**, *11*, 436. [CrossRef]
53. Kazmierski, M.; Glemas, P.; Rousseau, J.; Tisseyre, B. Temporal stability of within-field patterns of ndvi in non irrigated mediterranean vineyards. *J. Int. Sci. Vigne Vin* **2011**, *45*, 61–73. [CrossRef]
54. Ortuani, B.; Facchi, A.; Mayer, A.; Bianchi, D.; Bianchi, A.; Brancadoro, L. Assessing the effectiveness of variable-rate drip irrigation on water use efficiency in a Vineyard in Northern Italy. *Water* **2019**, *11*, 1964. [CrossRef]
55. Feng, M.; Yang, W.; Cao, L.; Ding, G. Monitoring Winter Wheat Freeze Injury Using Multi-Temporal MODIS Data. *Agric. Sci. China* **2009**, *8*, 1053–1062. [CrossRef]
56. Wang, H.; Huo, Z.G.; Zhou, G.; Wu, L.; Feng, H. Monitoring and forecasting winter wheat freeze injury and yield from multi-temporal remotely sensed data. *Intell. Autom. Soft Comput.* **2016**, *22*, 255–260. [CrossRef]
57. Gitelson, A.A.; Viña, A.; Ciganda, V.; Rundquist, D.C.; Arkebauer, T.J. Remote estimation of canopy chlorophyll content in crops. *Geophys. Res. Lett.* **2005**, *32*, 1–4. [CrossRef]
58. Gu, Y.; Brown, J.F.; Verdin, J.P.; Wardlow, B. A five-year analysis of MODIS NDVI and NDWI for grassland drought assessment over the central Great Plains of the United States. *Geophys. Res. Lett.* **2007**, *34*, 1–6. [CrossRef]
59. Heber, U. Conformational changes of chloroplasts induced by illumination of leaves in vivo. *Biochim. Biophys. Acta Bioenerg.* **1969**, *180*, 302–319. [CrossRef]
60. Ma, S.; Zhou, Y.; Gowda, P.H.; Dong, J.; Zhang, G.; Kakani, V.G.; Wagle, P.; Chen, L.; Flynn, K.C.; Jiang, W. Application of the water-related spectral reflectance indices: A review. *Ecol. Indic.* **2019**, *98*, 68–79. [CrossRef]
61. Wei, C.; Huang, J.; Wang, X.; Blackburn, G.A.; Zhang, Y.; Wang, S.; Mansaray, L.R. Hyperspectral characterization of freezing injury and its biochemical impacts in oilseed rape leaves. *Remote Sens. Environ.* **2017**, *195*, 56–66. [CrossRef]
62. Li, F.; Miao, Y.; Feng, G.; Yuan, F.; Yue, S.; Gao, X.; Liu, Y.; Liu, B.; Ustin, S.L.; Chen, X. Improving estimation of summer maize nitrogen status with red edge-based spectral vegetation indices. *Field Crop. Res.* **2014**, *157*, 111–123. [CrossRef]
63. Kasimatis, A.N.; Kissler, J.J. Responses of grapevines to shoot break-out following injury by spring frost. *Am. J. Enol. Vitic.* **1974**, *25*, 17–20.
64. Marcon Filho, J.L.; Allebrandt, R.; De Bem, B.; Mudrei, P.I.; Macedo, T.A.; Schlemper, C.; Lerin, S.; Outemane, M.; Kretzschmar, A.A.; Rufato, L. Damage to "Cabernet Sauvignon" after late frost in the Southern Brazilian highlands. *Acta Hortic.* **2016**, *1115*, 211–216. [CrossRef]

65. Bergqvist, J.; Dokoozlian, N.; Ebisuda, N. Sunlight exposure and temperature effects on berry growth and composition of Cabernet Sauvignon and Grenache in the central San Joaquin Valley of California. *Am. J. Enol. Vitic.* **2001**, *52*, 1–7.
66. Sadras, V.O.; Petrie, P.R.; Moran, M.A. Effects of elevated temperature in grapevine. II juice pH, titratable acidity and wine sensory attributes. *Aust. J. Grape Wine Res.* **2013**, *19*, 107–115. [CrossRef]
67. Jones, G.V.; Davis, R.E. Climate influences on grapevine phenology, grape composition, and wine production and quality for Bordeaux, France. *Am. J. Enol. Vitic.* **2000**, *51*, 249–261.